

Radar interferometry offers new monitoring approach for critical flood control infrastructure

Karen An¹, Cathleen Jones², David Bekaert², and Victoria Bennett³

¹University of California, Los Angeles

²NASA Jet Propulsion Laboratory

³Rensselaer Polytechnic Institute

November 23, 2022

Abstract

Aging flood infrastructure systems will need to be closely monitored as metropolitan areas globally face increasing inundation risk from sea level rise. To augment traditional ground survey, synthetic aperture radar (SAR) is shown to efficiently quantify elevation change along earthen levees with continuous spatial coverage. The study area, California's Sacramento-San Joaquin Delta, has an exemplar earthen levee system that protects the region from flooding. We investigate evidence of settling from historic levee breaks and small-scale subsidence features with a vertical velocity map and time-series of cumulative displacement derived from data acquired by the UAVSAR (Uninhabited Aerial Vehicle Synthetic Aperture Radar) L-band SAR, during 2009-2015. Comparison between radar and lidar maps (2007 and 2017) show that typical laser elevation surveys can miss subsidence features in the presence of normal maintenance activities. Historic levee break sites show more stable conditions due to the nature of repairs, and can be monitored using the SAR time series product. SAR information helps monitor the efficacy of repairs and targeted improvements to decrease the risk of levee breaks. In light of the upcoming NASA-ISRO SAR satellite mission, for which UAVSAR is the prototype, detailed monitoring will be attainable for levees worldwide.

Radar interferometry offers new monitoring approach for critical flood control infrastructure

Karen An¹, Cathleen E. Jones², David P. S. Bekaert² and Victoria Bennett³

¹ Department of Geography, University of California, Los Angeles, Los Angeles, CA 90095, USA.

² Jet Propulsion Laboratory, California Institute of Technology, Pasadena, CA 91109, USA.

³ Department of Civil and Environmental Engineering, Rensselaer Polytechnic Institute, Troy, NY 12180, USA.

Corresponding author: Karen An (karenan@ucla.edu)

Key Points:

- UAVSAR-derived map of cumulative elevation change identifies areas of anomalous and rapid subsidence close to critical levee infrastructure
- Large subsidence signals are hidden by levee repair work and maintenance in typical lidar surveys but measured by InSAR
- Time series product can be used to monitor historic levee breaks sites whose repairs result in more stability compared to surrounding

Abstract

Aging flood infrastructure systems will need to be closely monitored as metropolitan areas globally face increasing inundation risk from sea level rise. To augment traditional ground survey, synthetic aperture radar (SAR) is shown to efficiently quantify elevation change along earthen levees with continuous spatial coverage. The study area, California's Sacramento-San Joaquin Delta, has an exemplar earthen levee system that protects the region from flooding. We investigate evidence of settling from historic levee breaks and small-scale subsidence features with a vertical velocity map and time-series of cumulative displacement derived from data acquired by the UAVSAR (Uninhabited Aerial Vehicle Synthetic Aperture Radar) L-band SAR, during 2009-2015. Comparison between radar and lidar maps (2007 and 2017) show that typical laser elevation surveys can miss subsidence features in the presence of normal maintenance activities. Historic levee break sites show more stable conditions due to the nature of repairs, and can be monitored using the SAR time series product. SAR information helps monitor the efficacy of repairs and targeted improvements to decrease the risk of levee breaks. In light of the upcoming NASA-ISRO SAR satellite mission, for which UAVSAR is the prototype, detailed monitoring will be attainable for levees worldwide.

Plain Language Summary

The UAVSAR airborne radar instrument is used to study critical levee infrastructure that protects California's Sacramento-San Joaquin Delta from floods. This data is compared with typical laser elevation surveys that are used to monitor the area. Results show that the airborne radar is able to effectively measure large signals of subsidence, where the land is sinking, close

to the levees. The laser surveys, on the other hand, are unable to capture many levee subsidence features due to previous repair work that involved adding fill material. The time series of UAVSAR is also able to monitor levee conditions over time, showing fast settling immediately after a levee repair that eventually becomes more stable. UAVSAR is a prototype for an upcoming similar space satellite, so these results show the capability of radar remote sensing to help assess levee systems worldwide.

1 Introduction

With ten percent of the global population living in low elevation coastal regions (less than ten meters above sea level), coastal land loss will continue with more frequent flooding as sea levels rise (McGranahan et al., 2007; Tebaldi et al., 2012; Buchanan et al., 2016). Global extreme coastal water level exposure is estimated to affect 190 million people by 2100, three times as many people as previously estimated (Kulp et al., 2019). It is widely suggested that the sustainability of coastal areas will depend on engineered solutions (Tessler et al., 2015; Wuebbles et al., 2017). For example, in Manila, Philippines, there is a \$6 million flood management plan that includes building a new dam in an upper catchment area (The World Bank, 2017). Ho Chi Minh City, Vietnam has a \$4.4 billion project for tide control plans and building more dikes and reservoirs (Global Construction Review, 2016). Almost 400 km of higher seawalls have been erected in Japan since the 2011 Thoku earthquake and tsunami (Reuters, 2018). However, these structures may be built on compressible soils or areas already subsiding and will need continual monitoring. More than 70% of people currently exposed to permanent inundation or flooding live in Asian countries where there is a great need for data on the height and condition of levees and seawalls (Kulp et al., 2019). The importance of monitoring such coastal hazards is prioritized in the U.S. National Academy of Sciences' 2017 Decadal Survey for Earth Science and Applications from Space (National Academy of Sciences, 2018), which acknowledges the risk of increased storm activity to coastal areas protected by infrastructure to be a significant societal challenge.

Man-made levees are typically earthen embankments or concrete floodwalls, designed to divert the flow of water during a major flood event, storm surge, and seasonal high water (American Society of Civil Engineers, 2017). Even in areas where flooding is infrequent, and particularly those with dry climates, levees are often an integral part of a conveyance system that provides water to locations distant from the source. Sinking deltas such as the Ganges-Brahmaputra in Bangladesh, the second largest in the world, experience extreme sediment starvation from levees and dams built to combat flooding (Schmidt, 2015). The levees in Jakarta, Indonesia's largest city, are challenged by intense groundwater withdrawal that has accelerated clay compaction. In 2007, this led to catastrophic flooding in Jakarta, leaving 200,000 people displaced (Schmidt, 2015). In 2005, Hurricane Katrina caused catastrophic levee and floodwall failure in New Orleans, resulting in over \$200 billion in property damage and over 1 million people displaced (U.S. Army Corps of Engineers). In addition to protecting coastal cities, inland areas are often protected from riverine floods by levees. The United States contains an estimated 30,000 documented miles of levees, and up to 100,000 undocumented miles, with nearly two-thirds of Americans living in a county with at least one levee (American Society of Civil Engineers, 2017). In the U.S., 97% of the levees documented in the USACE National Levee Database are earthen structures, with the remaining 3% composed of

concrete floodwalls (American Society of Civil Engineers, 2017). The USACE Levee Safety Program accounts for levees that protect millions of people and \$1.3 trillion in property from flood damage, but the National Levee Database (NLD) received a "D" grade from the American Society of Civil Engineers' 2017 Infrastructure Report Card, indicating poor conditions based on engineering inspections and risk assessments. The grade shows a majority of the system experiencing significant deterioration at the end of their service life and large risk for failure (American Society of Civil Engineers, 2017).

Despite the importance of maintaining levees, methods of assessing their conditions remain largely ground-based with sparse spatial and temporal coverage, in most cases relying on day-to-day monitoring accomplished through visual surveys made by people driving or walking along the levees, augmented by measurements made at discrete locations (Weir, 1950; Broadbent et al., 1960; Prokopovich, 1985). Inclinometers and extensometers placed in bore holes are used to measure horizontal and vertical movement within the levee prism, and electromagnetic or seismic-based measurement identify the type of material within and beneath the levee (Rojstaczer & Deverel, 1993). Although modernized geodetic methods employing Global Position System (GPS) and Light Distancing and Ranging (LiDAR) are now used in many areas, theodolite surveys with or without electronic distancing capability are still used. All of the surveying methods commonly used for determining changes in the position of a levee or land surface rely on differencing surface contours measured at different times, which is limited by the precision and accuracy of the method employed. Furthermore, most methods are labor intensive, making it effectively impossible to obtain a continual long-term, regional view of levee conditions. Those methods that do allow more rapid acquisition over large areas, namely airborne lidar and orthophotogrammetry, have significantly poorer accuracy than can be achieved across smaller areas in ground-based surveys, so it can take many years to detect even relatively large velocities of 1-2 cm/yr or identify areas that are moving significantly relative to adjacent areas (Jones et al., 2016).

In contrast, it is possible to use a different remote sensing technique, namely synthetic aperture radar (SAR) interferometry (InSAR), to measure surface displacement directly across large areas at one time with far greater accuracy than is possible with traditional methods. InSAR satellite acquisitions are routine and can be used to measure how the structure is changing over time. In contrast, spaceborne lidars do not have the spatial resolution needed for levee monitoring (Markus et al., 2017), and airborne lidar surveys can be costly and hence infrequent. Differential interferometric synthetic aperture radar (DInSAR) allows for frequent and non-invasive measurements with centimeter to millimeter level precision (Amelung et al., 1999; Hooper et al., 2004). InSAR has been used previously to some extent for levee health monitoring (Jones et al., 2016), particularly making use of multiple polarizations of the radar pulses (Sehat et al., 2014), applying InSAR time series analysis in urban settings (Lanari et al., 2004; Chaussard et al., 2014), or being used to monitor the swelling and shrinkage of levees associated with meteorological conditions (Özer et al., 2019). The surface position surveys have largely used persistent scatterer InSAR (PSInSAR) to look at levees with hard surfaces and at a limited number of locations in urban areas (Dixon et al., 2006; Brooks et al., 2012). The main limitation is that short wavelength SARs (X, C band) experience rapid temporal decorrelation (Zebker & Villasenor, 1992), and so are challenged to detect small

movements or distinguish surface movement below vegetation, while the longer wavelength SAR instruments (L-band) available in the past have not had the resolution to image the levees directly. This limitation can be addressed with L-band instruments such as UAVSAR (Uninhabited Aerial Vehicle Synthetic Aperture Radar) (Fore et al., 2015), and the upcoming NISAR mission for a spaceborne L-band radar (Rosen et al., 2017).

In this study, an InSAR time series approach to monitoring the conditions of an earthen levee system in the Sacramento-San Joaquin Delta (“the Delta”) is evaluated and compared to airborne lidar-based monitoring. The Sacramento-San Joaquin Delta, the largest estuary in the western U.S. (4,800 km²), formed in the late 1800s as a freshwater tidal marsh east of the San Francisco Bay at the confluence of the Sacramento and San Joaquin Rivers. Drainage for agriculture has formed 65 low-lying islands surrounded by 1,800 km of levees (Service, 2007). However, these agricultural practices eventually led to ongoing land subsidence, mainly caused by aerobic microbial oxidation of soil carbon (Ingebritsen et al., 2000). Where land subsidence has reduced the island elevation below tide levels, the levees continuously hold back water, in contrast to more typical riverine levees that do so during high flow events. The aging levees effectively maintain the channel system that conveys fresh water to 3 million acres of farmland and part of the water supply for 25 million residents (Ingebritsen et al., 2000; Service, 2007).

A high resolution map of cumulative elevation change as a function of time is derived from UAVSAR data for the period 2009-2015. The ground settling rates at historic and recent levee impacts and breaks, and large subsidence signals across the Delta are complemented with a lidar differential of surveys from 2007 and 2017 (California Department of Water Resources, 2007; California Department of Resources, 2017). The Delta levees are a useful exemplar of other levee systems around the world because they are earthen embankments, typically constructed from compacted soil and covered with grass, gravel, stone, asphalt, or concrete to prevent erosion (American Society of Civil Engineers, 2017). An extensive network of drainage ditches that feed groundwater to pumping stations helps to prevent flooding, but levee breaks in the Delta have become commonplace in the last century (Deverel et al., 2016). Repair costs for these breaks range from \$43 to \$243 million and in some cases force total abandonment of the island (Bates & Lund, 2013). The Delta is also near many major seismic faults (Figure 1), with the San Francisco Bay region predicted to experience a 6.0 or larger earthquake at 98% probability by 2043 (Aagaard et al., 2016), putting the levees at risk of liquefaction (Deverel et al., 2016). Development of robust remote sensing methods for quantitative determination of earthen levee status, particularly those accessible at low cost and with global coverage, would have a significant effect on reducing risk to life and property throughout the world.

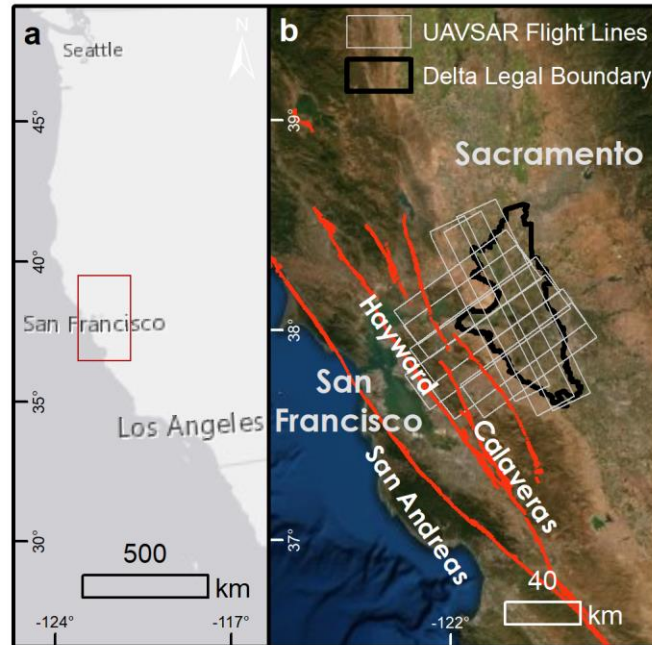


Figure 1. Overview of study area. The Sacramento-San Joaquin Delta is located in northern CA near many major faults (red lines). The coverage by UAVSAR is shown by the nine flight lines (grey polygons). In this study the SAR data are cropped to the legal delta boundary (black polygon) for overlap with the lidar surveys.

2 Materials and Methods

2.1 The UAVSAR Synthetic Aperture Radar

UAVSAR is a quad-polarized, L-band (23.8 cm wavelength) airborne synthetic aperture radar (SAR) instrument, flown in a pod carried by a NASA G-III aircraft. The instrument operates at an altitude of 12.5 km, with a bandwidth of 80 MHz and a center frequency of 1.2575 GHz. The image swath is 22 km wide, and the incidence angles range from 22° – 67° . The instrument spatial resolution is 0.8 m (along flight-line) by 1.7 m (along the line-of-sight (LOS)) (Bekaert et al., 2019). The longer wavelength, high spatial resolution, and flexibility in acquisition geometry make UAVSAR an advantageous instrument for monitoring levee systems. Nine flight lines cover the majority of the legal Delta boundary (Figure 1). Each line was acquired between 52 to 60 times from July 2009 to October 2015. To minimize artifacts due to aircraft motion, the aircraft is actively controlled to stay within 5 m of the planned flight path. During post-processing image offsets are determined, the flight track is corrected, and the datasets are re-processed. Using measurements of aircraft position and 3-D acceleration during post-processing achieves 8 mm precision, but residual position errors of 0 to 5 cm can persist in the image. These artifacts can appear as linear ramps perpendicular to the flight direction, which are removed in processing, or bands in the along-flight direction. The latter are not removed but are reduced by averaging in the InSAR time series processing. InSAR only measures surface displacement in the line-of-sight direction, so having multiple look directions eliminates the effect of levee orientation on monument sensitivity.

2.2 LiDAR Surveys

The California Department of Water Resources (CA DWR) conducted two lidar surveys over the Delta 10 years apart, in 2007 and 2017. The most common use of lidar is to generate high precision digital surface models, which can be used to study forest canopy structure, archaeological sites, and landslide risk (Dubayah & Drake, 2000; Chase et al., 2012; Jaboyedoff et al., 2012). Lidar is able to measure surface changes such as subsidence between two events, but if the surface has material added, lidar will measure the net of all sources of elevation change. Elevation was collected at 0.5-1-meter spacings (vertical datum NAVD88, geoid model Geoid03 Continental US). For the 2007 survey, the vertical accuracy was calculated to be 15 cm at 90% confidence and less than 18.5 cm at 95% confidence (California Department of Water Resources, 2007). For the 2017 survey, the measured vertical accuracy was 10.7 cm at 95% confidence level (California Department of Water Resources, 2017). A differential was calculated between the surveys to compare with the InSAR time series cumulative displacement, which was collected over a shorter time period, 2009-2015, with more frequent measurements. The differential was calculated as the 2017 elevation minus the 2007 elevation, and divided over 10 years, hereafter known as lidar vertical velocity. Since there are only two data acquisitions, the rates calculated should not be considered linear over the time period, but rather an indicator of average cumulative change between two snapshots in time.

2.3 GPS Data

On one of the most critical Delta islands, our team commissioned GPS (Global Positioning System) stations to measure elevation changes from April 2015 to July 2017. Three stand-alone continuously monitoring GPS stations were installed along the setback levee on Sherman Island in April 2015. These stations were anchored to the ground surface using a 3-foot deep concrete pedestal. The locations of the GPS stations are shown in Figure 2C. Each station contains a Novatel ProPak 6 receiver and a dual-frequency GPS plus GLONASS pinwheel antenna. The ProPak 6 is a high performance Global Navigation Satellite System (GNSS) receiver capable of tracking different combinations of GNSS signal and integrated L-Band on 240 channels. The receivers have a built-in cellular modem and are connected to the ATT network for remote data transmission. The reference frame was NAD83CSRS and the raw GPS data time series for each station can be found in the supplementary material in Figure S1. The GPS station data was also normalized and projected into the line-of-sight for more direct comparison with the InSAR product's time series for individual flight lines. This conversion is based on the decomposition of the east-north components of a UAVSAR flight line. See Figure S2 in the supplementary material for details.

2.4 UAVSAR Time Series Processing

The first spatially comprehensive map of modern subsidence rates (vertical velocity) in the Delta was reported in Bekaert et al. (2019). The reported vertical velocities show the Delta to be subsiding by 9.2 ± 4.4 mm/yr on average in 2009-2015, with high variability across islands. The same UAVSAR dataset is utilized for this study, but clipped and smoothed along the levees for a separate analysis. The time series

product, with values for each acquisition date, is used to present the plots of cumulative displacement over time, and the vertical velocity map is used to visualize the spatial patterns of subsidence. Included below is a summary of how the vertical velocities were generated, with full details in Bekaert et al. (2019).

Using the Small Baseline Subset (SBAS) time-series processing algorithm (Berardino et al., 2002) and the GIANt toolkit (Agram et al., 2013), the cumulative LOS (line-of-sight) displacement time series and uncertainty are calculated from unwrapped interferograms. The derived displacements are relative to different reference points for each flight track, with the reference location selected based on high coherence and amplitude/phase stability. In the process of combining the data together to form a single map, the InSAR results are re-referenced to 24 GNSS stations within the scene extent as a tie-in for the mosaicked flight swaths. The GNSS products used are from the Nevada Geodetic Laboratory and have horizontal rate uncertainties up to 0.3 mm/yr (Blewitt et al., 2013). Consistency is required in the swath overlap regions to solve for reference corrections in a single inversion strategy. Broad-scale horizontal movement from nearby faults is removed from the rates. For the final combined map, the GNSS rates are used to remove long wavelength artifacts (ramps, tilts), while the InSAR rates constrain local variability. By implementing a planar correction for each flight line when constraining the flight swath overlap regions, tropospheric delay and residual position errors are further reduced. Vertical velocity maps from the different flight lines are combined with a weighted average, allowing areas with overlapping pixels to have lower uncertainty. The corresponding uncertainties are calculated using a jackknife approach. A full propagation of errors is included, with an RMSE of 7.7 mm/yr between GNSS rates and the vertical velocities. See Figure S3-S4 for the vertical velocity and uncertainty maps for the major central Delta islands obtained from Bekaert et al. (2019).

Atmospheric corrections were also applied using the ERA-Interim global atmospheric model (Doin et al., 2009) using a modified version of the TRAIN toolbox (Bekaert et al., 2015). The modifications made were to integrate the refractivity from the surface to the aircraft altitude and incorporate time-of-day of acquisitions. Localized systematic noise from ground fog or low lying clouds was also considered. Monthly temperatures from Sacramento were used to estimate atmospheric delay from 100% humidity at 1 km above the ground (Younes, 2016), and the values ranged from 0.63 to 2.10 mm, which is well within the estimated accuracy of the data.

To evaluate whether the residual of the InSAR and lidar vertical velocities (v_{InSAR} and v_{LiDAR} , respectively) is larger than the uncertainty, the following expression was applied:

$$|v_{InSAR} - v_{LiDAR}| \leq \sqrt{\sigma_{v_{InSAR}}^2 + \sigma_{v_{LiDAR}}^2} \quad (1)$$

where $\sigma_{v_{InSAR}}$ is the 1-sigma uncertainty calculated for the InSAR vertical velocities (as stated above) and $\sigma_{v_{LiDAR}}$ is 10.7 mm/yr, which is the 1-sigma uncertainty as calculated from the vertical accuracy reported from the lidar datasets (California Department of Water Resources, 2007; California Department of Water Resources, 2017). If the expression is true, then the InSAR and lidar vertical velocities measured are consistent within the datasets' uncertainties. Across the entire Delta legal boundary, where there are

both lidar and SAR data, 99.8% of pixels showed agreement (see Figure S5 for the visual comparison of these results and Bekaert, et al. (2019) for scaling information).

2.5 Levee Oriented Moving Window Average

A collection of GIS (geographic information systems) datasets was used to investigate the results of the InSAR and lidar vertical velocity maps: levee anatomy (CA DWR), historic levee breaks (CA DWR), and repair and seepage locations (CA DWR). The levee anatomy vector datasets differentiate portions of the levee as the levee crown, levee landside and waterside slopes, and toe ditch and berm. The final map of vertical velocity was clipped to the boundaries of this combined anatomy to isolate the values for the levees only. Past levee break locations provided by the DWR are used to identify areas that could be settling after repair work. The levee anatomy layer was used to mask the InSAR vertical velocity map in Esri's ArcMap 10.6. Next, equally spaced points were generated along the levee crown/centerline and visually inspected for accuracy for each island. These points were indexed and used to calculate a moving window average of the vertical velocities. Each window is uniquely generated by searching for the nearest points along the waterside levee and landside levee boundaries. A best-fitting window is generated for each levee centerline point. This is done to ensure that a consistent length of the levee is averaged at each step, between 70-100 m. Unlike a traditional moving window, the generated window is levee-oriented, i.e., it modifies its orientation with respect to a levee's location on an island. Since the levee's landside and waterside slope vary in width and shape across an island, a static window would not capture the actual levee section for all locations. For more details, see Figure S6 in the supplementary material. This moving average window is used to reduce noise in the dataset, while retaining the major patterns of the original velocity map. Both the vertical velocity and the uncertainty estimates were calculated with the adaptable sliding window.

3 Results, or a descriptive heading about the results

The average vertical velocities on the levees within the Delta legal boundary range from -77 to 14 mm/yr, showing high variability island to island. Below, the largest subsidence signal in the Delta is presented alongside GPS station data and the lidar vertical velocity map. Other subsidence signals in the Delta are also investigated, and the rates of settling between historic and recent levee breaks and impacts (where the levee was struck by a vessel) are also compared with the lidar surveys.

3.1 Levee Subsidence

The section of levee showing the highest rates of subsidence across the Delta is located in southwestern Sherman Island, with up to -160 mm/yr of subsidence (Figure 2A). The full resolution from the unsmoothed vertical velocity map is shown in Figure 2A, and the smoothed levee-specific results in Figure 2C. From the smoothed results, it can be seen that one portion of the levee is experiencing the highest rate of subsidence, and this rate gradually decreases on either side of the section. Nearby this section is the 1969 levee break, indicated in Figure 2A-C southeast of the subsidence feature, which shows more stable conditions consistent with levee sections further from the location of maximum rate. Figure 2B shows the lidar vertical velocity results for the same area. Lidar shows a large increase in elevation that coincides spatially with the highest subsidence

signal from the InSAR results. Independent of auxiliary information, one would infer from the lidar data that no subsidence was occurring at this location. In fact, the elevation increase is likely due to the continual addition of fill to maintain the elevation in this area.

The large subsidence signal is also confirmed by three GPS stations from our team, the locations of which are shown in Figure 2C. The smoothed InSAR results and the InSAR LOS time series of the three GPS locations (Figure 2D), shows that Station 1 and 2 have the higher rates of displacement compared with Station 3. Comparing this to the projected LOS rates for the GPS station data (Figure 2E), Station 1 also has the highest cumulative displacement. Station 2 has a very similar InSAR LOS time series to Station 1, but is closer to Station 3 when looking at the GPS LOS time series. In both datasets, Station 3 shows the least amount of vertical displacement.

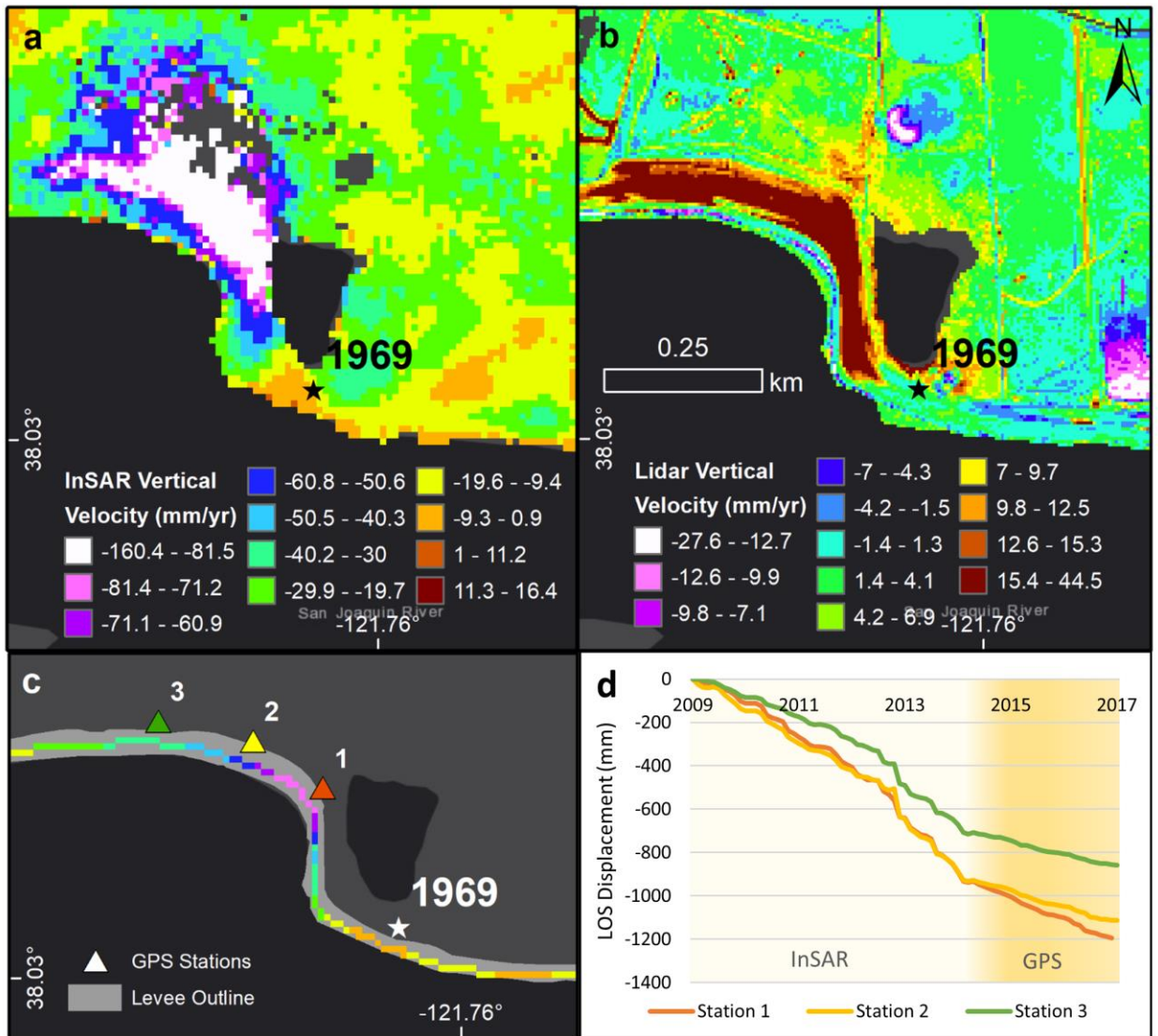


Figure 2. Levee subsidence on Sherman Island. (a) Vertical velocity map for southwestern levee section showing the greatest subsidence in the Delta, and a stable

1969 levee break. **(b)** Lidar vertical velocity for the same section showing large elevation gain. **(c)** Smoothed results of panel a showing levee outline (grey) that the moving window was applied to, and the three GPS stations (colored triangles). **(d)** LOS displacement from InSAR time series product for the GPS station locations for 2009-2015 and GPS time series for the three stations converted to LOS displacement for 2015-2017.

Some other major subsidence signals across the Delta are shown in Figure 3. In Figure 3A, there is a long stretch of subsidence along the northern section of Webb Tract that matches exactly with the elevation gain seen in the lidar vertical velocity map in Figure 3B. From the original InSAR rate map, Figure 3A shows these large subsidence signals in close proximity to the levee. The largest subsidence feature on the west measures up to -56 mm/yr. Like the Sherman Island example, the InSAR measures actual deformation at the surface while the lidar shows an elevation gain at the same site. Known repair work occurred along this levee section for toe ditch cleaning and seepage control. On Jersey Island (Figure 3C), a large signal of up to -47 mm/yr of subsidence is seen close to the levee with another large subsidence feature more inland. In this case, the lidar surveys in Figure 3D agree with the InSAR results and also show significant elevation loss. The features are not identical, but both datasets show the highest rates of subsidence close to the levee and extending inland. For a different section of Sherman Island shown in Figure 3E-F, three large subsidence features close to the levee are shown. These features also show up as elevation loss in the lidar data in Figure 3F, with the easternmost example exhibiting the highest elevation loss in both the InSAR and lidar, up to -48 mm/yr.

As discussed in the Methods section, a measure of sensitivity for the InSAR and lidar residuals against their uncertainties was evaluated. For the scaled $\sigma_{v_{InSAR}}$ sensitivity result (Figure S5), when only looking at the central islands (as shown in Figure S3-S4), 0.17% of pixels for island interiors disagreed in sensitivity while 2.45% of pixels for the levees disagreed in sensitivity. This indicates that the InSAR and lidar datasets are more than 14 times as likely to be out of each other's uncertainty bounds on the levees as on island interiors. Areas of disagreement coincide with large InSAR subsidence features like on Sherman Island that are masked by repair work's elevation gain in the lidar vertical velocity map.

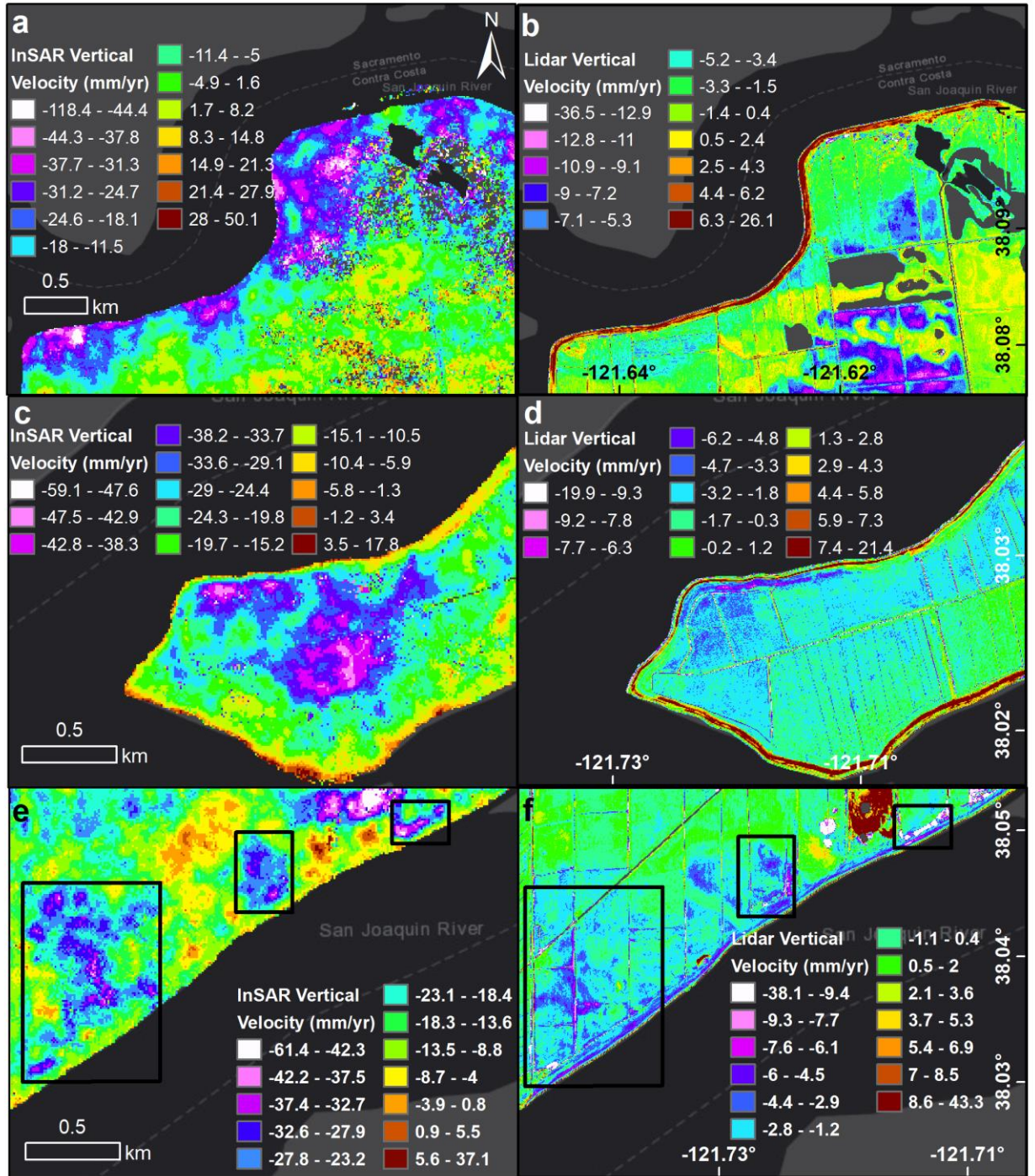


Figure 3. Levee subsidence on other islands. (a) Vertical velocity map showing subsidence along northern section of Webb Tract. (b) Lidar vertical velocity of same section of Webb Tract. (c) Vertical velocity map showing subsidence on Jersey Island. (d) Lidar vertical velocity of same area on Jersey Island. (e) Vertical velocity map of three large subsidence features along south section of Sherman Island. (f) Lidar vertical velocity of same area on Sherman Island.

3.2 Historic Levee Breaks

In Figure 4, sections of four Delta islands that are the sites of past levee breaks are shown. At each of these sites, the area of previous repair of a levee break is evident in the velocity map as being more stable than its surroundings. These rates differ between the three examples, from -2 up to 8 mm/yr, but relative to each location's surroundings, the levee break point shows the least amount of subsidence. For each location, the subsidence rates increase gradually as you move away from the levee break point on either side. This is likely due to the method used for levee repairs, in which solid material such as rocks or fill are added to the levee break site and also extend to unimpacted levee on both sides. Over time, this material, depending on its contents, begins to settle and becomes more stable. As seen in Figure 4B-D, scour (or blowout) ponds directly adjacent to the breaks were formed during flooding, as water scooped up layers of peat and penetrated island interiors deep enough to maintain permanent seepage (CALFED Bay-Delta Program, 2000).

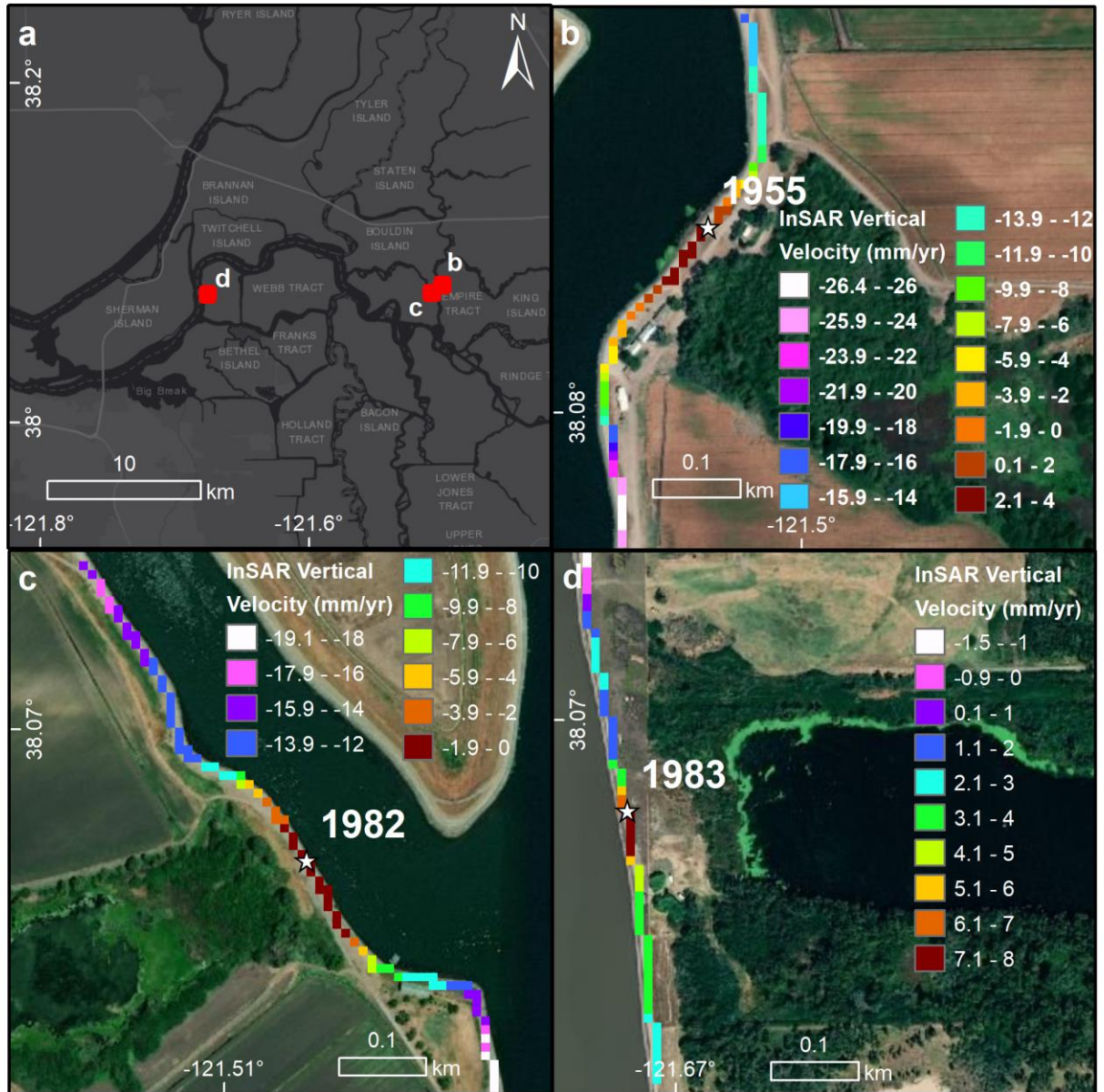


Figure 4. Historic levee breaks. (a) Overview of central Sacramento-San Joaquin Delta islands. (b) Vertical velocity map showing stable conditions at a 1955 break on Empire Tract. (c) Vertical velocity map showing stable conditions at a 1982 break on Venice Island. (d) Vertical velocity map showing stable conditions at a 1983 break on Bradford Island.

The most recent levee break occurred in 2004 on Jones Tract, as seen in Figure 5. In the optical imagery basemap, a large land scar inland also shows the path of flooding that occurred during this massive event. At the break point, the InSAR-derived rates measure -8 to -6 mm/yr of settling, which is much higher than those for the older break sites shown in Figure 4, likely due to this levee break being fairly recent in time. Like the other levee break examples in Figure 4, Jones Tract also displays a similar pattern of gradually higher subsidence/settling rates moving away from the break location.

However, here the pattern is not as smooth with large sections of the levee showing high rates of settling, up to -14 mm/yr on the western side and -9 mm/yr on the eastern section. In Figure 5B, the lidar vertical velocity between 2007 and 2017 is shown for the Jones Tract break. Here, a larger value means that the elevation has increased from 2007 to 2017, which is seen in the red pixel sections on either side of the break point. At the break, there is an elevation change of -2.6 mm/yr to 0.6 mm/yr, and on either side of the break, an elevation increase of up to 24 mm/yr.

This location of pattern is coincident with the settling pattern seen in the InSAR, but with opposite trends in elevation change. Due to repair work adding material, InSAR settling (negative value) is observed as lidar elevation increase (positive value). The lidar surveys measure net elevation change, including added fill material between acquisitions, and not the ongoing settling since the repairs were administered. In fact, where the InSAR shows the least amount of settling at the break site, the lidar shows less elevation gain. On either side of the break where InSAR shows faster rates of settling, the lidar shows more elevation gain. Although the west side of the impact shows more subsidence from InSAR, it has less elevation gain in the lidar compared to the east side of the impact. It is confirmed in Google Earth that extensive repair work occurred in this area, especially on the eastern side, between October 2011 and May 2012 that matches the elevation gain features seen in the lidar. This may also explain the trend seen in Figure 5C of increased displacement around 2011-2012 for the area. This breach on Jones Tract flooded the island with over 150,000 acre-feet of water and required 3 weeks for repair, costing about \$90 million to repair, with the actual repair costing \$30-\$40 million and the remaining costs for property damage (U.S. Army Corps of Engineers; Deverel et al., 2016).

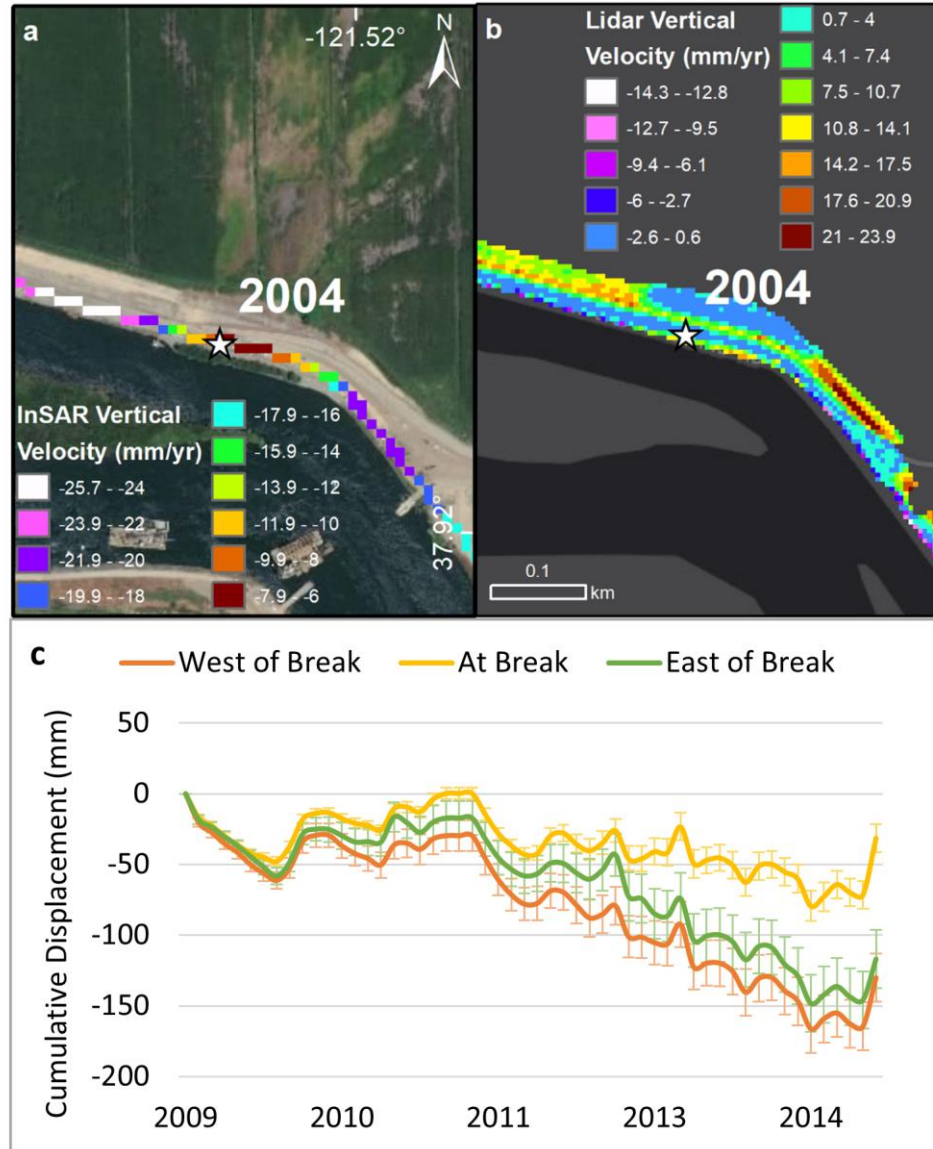


Figure 5. Most recent Delta levee break. (a) Vertical velocity map showing stable conditions at 2004 levee break on Jones Tract with flood scar inland. (b) Lidar vertical velocity showing high elevation gain on either side of break site. (c) LOS displacement from InSAR time series product for pixels to the west, east, and at the break site from 2009-2015.

3.3 Levee Settling Immediately After Repair

On August 27, 2009, a 175 m bulk carrier ship collided into the north side of Bradford Island, damaging 45 m of the levee with significant cracks. Figure 6A shows an optical image one month after the impact, with repair work indicated by the bare earth section of the levee. In the InSAR results shown in Figure 6C, this repaired section is experiencing rapid settling, with rates from -19 to -31 mm/yr. Here, the opposite pattern is seen from the historic levee break examples, where at the impact site the highest rate of settling is seen, and with rate decreasing on either side. Over time, the reverse trend should be expected with the repair site showing the most stable rates. The trend is seen in

the InSAR LOS time series in Figure 6B, where pixels at the impact site are experiencing more displacement than its surroundings. There is an initially high rate of settling for the whole area between 2009 and 2012, relative to later years. The lidar vertical velocity map in Figure 6D shows an elevation increase at the repair site that is also apparent at older levee break sites, but with a higher rate of 42 mm/yr since the initial repairs occurred in 2009 between the lidar acquisitions. We also see a section of elevation loss in Figure 6D west of the impact site that corresponds to higher subsidence rates in Figure 6C and is outside of the repaired levee section.

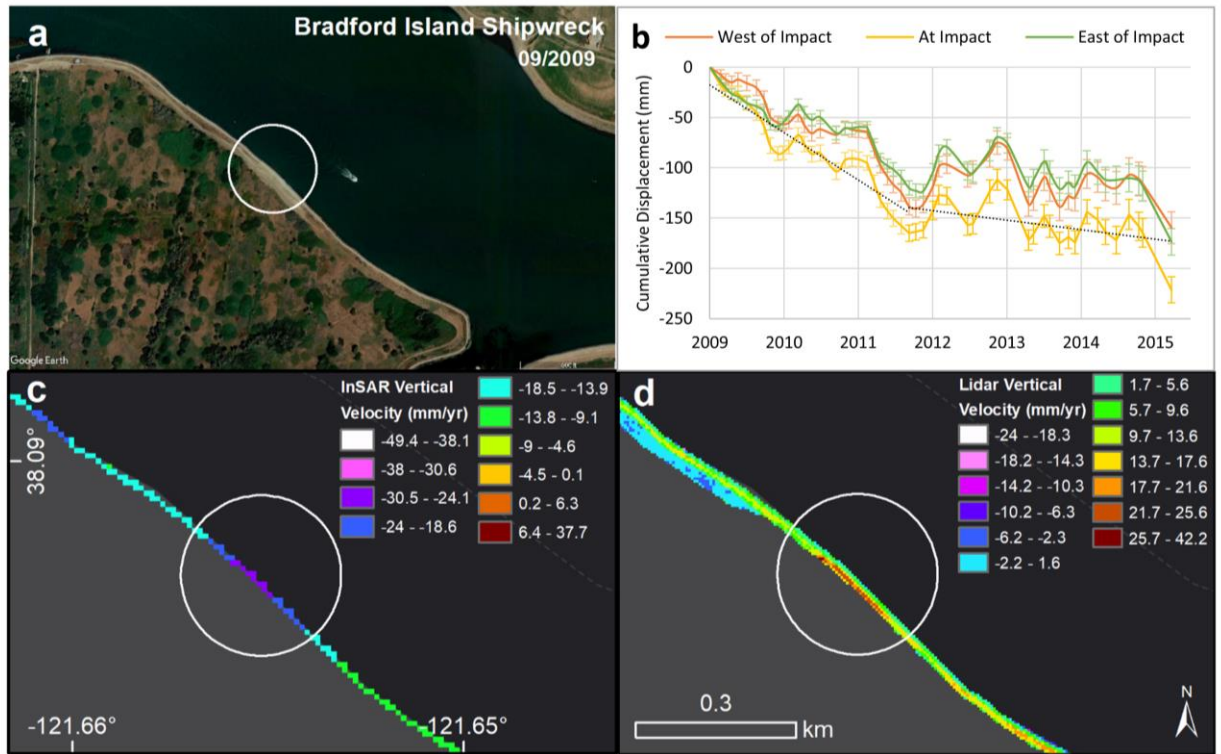


Figure 6. Recent levee impact. (a) Google Earth image of Bradford Island one month after shipwreck impact (circled). (b) LOS displacement from InSAR time series product for pixels to the west, east, and at the impact site from 2009-2015. (c) Vertical velocity map showing high subsidence values at the impact site. (d) Lidar vertical velocity map showing high elevation gain at the impact site.

4 Discussion

Like the levees enclosing New Orleans, the Sacramento Delta levees are under constant hydrostatic stress even between high water events because the islands lie beneath mean sea level. A measurable indicator and predictor of levee conditions in the Delta relevant to water resource management is land subsidence on or near a levee, which can be highly spatially variable, depending on soil characteristics and land practices. The largest contributor to land subsidence in the Delta is microbial soil oxidation, especially for dry peat soil used for agriculture in island interiors. However, for the levees, the structures sit atop these soft, compressible peat layers and experience subsidence, or settlement, primarily from consolidation and secondary compression. The added force

from the levees causes water to be squeezed out of the soil, a slow process due to the low hydraulic conductivity of the peat (Reinert et al., 2014).

The InSAR-based methodology presented here can be used to quantify contemporary subsidence rates in a spatially comprehensive and consistent manner independent of levee orientation. High resolution levee monitoring allows for managers to focus traditional surveys on sections of the levee most likely to be experiencing subsidence. The centimeter-to-millimeter level displacement accuracy can also detect precursors to levee failure unidentified by typical visual inspections.

4.1 Levee Subsidence

Sherman Island is the westernmost island in the Delta, and thus helps control the salinity gradient between brackish water entering from the San Francisco Bay and freshwater resources to the east. In 1972, a levee failure on an adjacent island, Brannan, caused a salinity intrusion that stopped water exports from the Delta, and over 350 million m³ of freshwater was released from reservoirs to reduce saline conditions (Deverel et al., 2016). Sherman Island was one of the earliest reclaimed islands in the late 1800s, and today is mostly pasture area, with some active corn and alfalfa sites (Boryan et al., 2011). This island has experienced five major inundation events since 1900 and two levee breaks, one of which is shown in Figure 2. The 1969 break site is the more stable stretch of levee due to the method of repair. First, rocks were used to fill the break, which do not experience the same compression as only adding fill material. Later in 2007, the levee was broadened and more fill material was added at this site. Knowing the settling rates in between these two repairs would be helpful when adding sufficient material to maintain levee height after the initial rapid settling.

The largest signal of subsidence in the Delta is observed on Sherman Island at the test site, measuring up to 160 mm/yr. This subsidence signal is also confirmed by the GPS stations, which show Station 1 having the largest displacement trend. Both the InSAR and GPS time series show Station 1 having the highest displacement and Station 3 measuring the least. The GPS stations are also located more inland (outside the levee mask), and may not be capturing the full extent of deformation occurring on the levee structure itself. GPS time series data are needed as ground-truth for the InSAR product, but only capture movement at a single point, and an extensive network of stations across all islands is not feasible. This comparison demonstrates the need for continual SAR data collection over the Delta. The large subsidence feature also coincides with the lidar data in Figure 6 showing a large increase in elevation, up to 45 mm/yr, of repair work. If relying solely on decadal lidar surveys, the vertical velocity would not measure settling in any area where fill was added, i.e., would be sensitive to repair work, whereas an InSAR time series product as processed in this study shows actual subsidence. Since radar backscatter is sensitive to changes in surface roughness and dielectric properties, if fill material is added there would be a loss of coherence in the SAR data due to the difference in material (Jones et al., 2016). Low coherence pixels are not included in the time series processing, and thus the final vertical velocity map is a result of acquisitions showing true surface movement (subsidence/uplift). As shown in Figure 2D, multiple acquisitions allow for continual measurements of such sites experiencing intense subsidence. Especially for areas where the land behind the levee lie significantly below

mean sea level, such as islands in the central Delta, knowledge of ongoing subsidence rates for the levees is critical for administration of maintenance resources.

In Figure 3, Webb Tract showed a similar result to Sherman Island, with elevation gain in the lidar and elevation loss in the InSAR. Again, a large subsidence signal is being masked by repair work in the lidar vertical velocity map. Therefore, lidar cannot be the sole survey used when measuring elevation change to identify at-risk levees in areas with ongoing maintenance. Where there is major subsidence but not extensive repair work, lidar does agree with elevation loss in the examples on Jersey and Sherman Island. At both sites, the lidar matches well with the InSAR for the location and intensity of large subsidence features. However, it can be argued that areas receiving repair work have been deemed a priority by levee managers, and thus especially need settling rate information. It is promising that UAVSAR is able to identify subsiding levees, especially in such a coherence challenged area such as the Delta, regardless of ongoing addition of fill material on the levees. The location of such large subsidence features can be communicated to levee managers as possible points of vulnerability that require further inspection.

4.2 Levee Settling After Repairs

With about 160 levee breaches in the past century and repairs costing tens of millions of dollars, close monitoring of levee conditions vulnerable to breaches is vital (Bates & Lund, 2013). Levee failure usually occurs during a high water event that causes overtopping or erosion, but can also occur during a normal day from internal degradation due to an ongoing seep, slumping, cracking, or animal burrowing. Close monitoring of areas in proximity to previous levee breaks (e.g., Figure 4) is important since these levee sections have already proved to be vulnerable in the past. Though these sites do not seem to be subsiding currently, the repairs are often made atop less stable levees or compressible peat and sandy soils, and the surrounding area for each levee break do show subsidence based on our results.

As seen from the results, observations of subsidence initially following repairs are more likely temporary loading on organic soils from the addition of fill during the levee repair. For the most recent levee break in the Delta (Figure 5), this short-term settling is especially apparent when compared to older levee breaks, with rates up to 24 mm/yr, whereas the 1955 break on Empire Tract is only settling up to 4 mm/yr. The same pattern of more stable breaks is seen at 20 different locations across the Delta (see Figure S7 in the supplementary material). Having such information about levee break locations allows differentiation between temporary settling from a repair and ongoing, long-term subsidence. Over time, repair tactics have also changed, and depending on the material added, the repaired break may show different rates of settling. Continual InSAR satellite measurements over a levee system can help identify subsiding sections before a levee breaks or overtops, and let water managers know areas most susceptible to failure. After a repair, InSAR can help evaluate the efficacy of the repair method by measuring the rate of settling from different materials being added. Depending on the underlying soil, the response to loading from the fill material will vary for different sites.

In 2009, a shipwreck occurred on Bradford Island 12 days before the start of the InSAR time series, resulting in serious cracking of the levee. The levee portion did not break due to immediate repair work of adding sand, silt, and clay to stabilize the levee.

Since this event occurred close to the start of the InSAR time series, it allows for the observation of initial rates of settling after the repair, up to -30 mm/yr, the largest value of all the historic levee break examples in this study. This indicates that rates of settling are highest directly after a levee repair and begin to decrease over time on a timescale of approximately three years. Such information can benefit levee managers in monitoring an administered repair to ensure that the settling that occurs is short-term and does not indicate long term subsidence for an already vulnerable area.

This monitoring method can be applied to other levee systems as well with the launch of NISAR. A similar analysis was conducted using UAVSAR-derived vertical velocities in New Orleans, LA (Jones et al., 2016). Here, levees that also protect from high water events such as the Bonnet Carré Spillway, Mississippi River-Gulf Outlet Canal showed concerning rates of subsidence. The levees near the Michoud Canal, which lie near the Inner Harbor Navigation Canal Surge Barrier, showed the maximum subsidence in the scene, up to 50 mm/yr. The potential of UAVSAR and NISAR to be used during emergency response will greatly aid the direction of resources after a large flood or earthquake (Rosen et al., 2017). For day-to-day monitoring, the detection of small deformation features along the levee can lead to timely assessments before actual levee failure occurs. The results show that such InSAR time series products can measure long term deformation from subsidence, seasonal changes due to temperature and precipitation, and short term deformation from settling. These various timescales allow for detection of a variety of levee behaviors, such as long term uplift that can lead to piping, short term deformation from a high water event, and long term drought periods that can cause levee sliding (Özer et al., 2019).

4.3 Uncertainties & Challenges

Measuring deformation in a study area such as the Delta can be challenging, even with an L-band SAR instrument. There can be data processing errors from decorrelation of the baseline, temporal terrain decorrelation, co-registration errors, or noise from volume scattering in vegetation (Hanssen, 2001). Systematic errors can arise from aircraft motion, tropospheric delay in the atmosphere, or land use change. Disturbances on the surface caused by farming activity (grazing, cultivation, etc.) can cause temporal decorrelation (Deverel et al., 2016). The time series methodology used with the SBAS technique generally averages out atmospheric noise during analysis, with random noise usually being reduced by the square root of the number of acquisitions. Each of the nine Delta stacks had over 50 acquisitions. UAVSAR also imaged the Delta at different times of day and over different seasons over six years, which would randomize the atmospheric noise.

Spaceborne radar satellites will experience most of the same challenges but with a higher noise level and a sensitivity to levee orientation since there will only be two look directions, namely from the ascending and descending paths. However, the instrument will have a more consistent repeat cycle and shorter acquisition interval that can allow for longer time series products to be produced with maintained coherence. Having regular and frequent acquisitions will allow for the differentiation between short-term settling, seasonal changes, and land subsidence in dynamic deltas where levees experience frequent repairs. A common method to study man-made infrastructures such as dams or bridges is PSInSAR, but the coherent scatterers are usually found on surfaces without

vegetation. For deltas with high agricultural activity and wet conditions, this means that PSInSAR scatterers would likely only be found along the waterside rip-rap slope of the levee, and not on the levee crown or land-side slope where subsidence can have different rates (Özer et al., 2019). The upcoming NISAR satellite will have longer wavelength than others in operation (L-band) that can help to improve coherence for such deltas and increase data coverage.

5 Conclusions

This study shows the feasibility of high resolution monitoring of a levee system using an L-band radar instrument, and contrasted InSAR- and lidar-based methods. The SAR and lidar observations are not always measuring the same physical process, with levee repair work in the lidar data often masking large subsidence signals seen in the SAR data. Though the lidar surveys offer high-resolution elevation data, they were shown to detect elevation gain at levee repair sites due to the addition of fill material. With a priori knowledge of repair sites, the InSAR time-series method is able to differentiate between short-term settling after a levee break and ongoing subsidence.

Some subsidence reversal may be possible through land-use practices that increase sediment accumulation or natural accretion in protected marshes (Bates & Lund, 2013). However, the “patch and pray” method of repairs is unsustainable, and so implementing InSAR-derived deformation detection can help targeted repair of levee locations showing initial signs of failure. In the face of climate change, there is likely to be less winter snow and earlier spring snowmelt in California and precipitation decreases in southern California, causing greater dependence on groundwater (Luoma et al., 2015). Due to this water supply uncertainty, California water demands from the Delta are likely to increase in the future while water availability from the Delta will decrease and gain economic value (Lund, 2016). More frequent drought periods for California are also of concern since a levee break during a dry year will be more detrimental to the water supply. The U.S. has many levees non-compliant with standards, for which subsidence will worsen levee integrity. Using local tide gauge data, Bekaert et al. (2019) estimate that on average, subsidence rates in the Delta are a factor of 4.5 higher than sea level rise rates, which absent continual and increasing repairs likely result in more overtopping events in the Delta and increase erosion along the levees.

The method demonstrated is generally applicable for other deltas and low-lying coastal areas, protected by levees and flood-walls. With almost half a billion people living on or near deltas in the world’s largest cities, the risk of coastal flooding and loss of infrastructure is ever imminent (Syvitski et al., 2009). The 10 million people a year that experience storm surge flooding live mostly on deltas in Asia from heavy precipitation and storms (Syvitski et al., 2009). In the coming decades more metropolitan areas will come under threat of flooding, possibly adding sea walls and levees as defense against sea level rise (Tessler et al., 2015; Wuebbles et al., 2017). These structures will be built upon compacting soils with reduced aggradation (common in deltas due to drainage or oil/gas extraction), and need continuous monitoring to maintain their integrity (Syvitski et al., 2009).

UAVSAR is the prototype for the upcoming NISAR satellite from NASA-ISRO, and this study previews the capability of the spaceborne L-band satellite to study similar levee systems around the world. NISAR will image at instrument resolutions of 6-12

meters, with products available 1-2 days after observation and possibly within hours for disaster response (Rosen et al., 2017). Since NISAR is dual-polarized, utilization of the polarimetric radar (PolSAR) methods can amplify detection of levee vulnerabilities such as seepage (Sehat et al., 2014). In addition, automated creation of deformation maps for vulnerable levee systems will be more feasible with increased global and temporal coverage to identify anomalous conditions. As shown in this study, the technology has the capability of monitoring critical infrastructure before, during, and after a disaster event. Especially in areas of the world where traditional surveying is sparse or expensive, SAR remote sensing can offer detailed measurements crucial to the health of the levee system.

Acknowledgments, Samples, and Data

The authors thank Joel Dudas from the California Dept. of Water Resources for important information about the Sacramento-San Joaquin levee system. The authors also thank Yongwei Sheng and Scott Brandenburg from UCLA for their helpful comments. The authors acknowledge the GNSS community for maintaining the GNSS/GPS networks and the UAVSAR team for acquiring and processing the data into SLC stack products. This material is based upon work supported by the NASA Earth and Space Science Fellowship. This work was also supported in part by the Jet Propulsion Laboratory, California Institute of Technology, under a contract with the National Aeronautics and Space Administration. Funding for data acquisition and analysis was also supported in part by the California Dept. of Water Resources and the Dept. of Homeland Security. Any use of trade, firm, or product names is for descriptive purposes only and does not imply endorsement by the U.S. Government. The lidar surveys can be accessed through the California Department of Water Resources GIS archive (see references). The UAVSAR vertical velocity rates and corresponding uncertainties can be found at <https://data.caltech.edu/records/1370>.

References

- Aagaard, B. T., Blair, J. L., Boatwright, J., Garcia, S. H., Harris, R. A., Michael, A. J., et al. (2016). Earthquake outlook for the San Francisco Bay region 2014–2043 (Tech. Rep.). doi: 10.3133/fs20163020
- Agram, P., Jolivet, R., Riel, B., Lin, Y., Simons, M., Hetland, E., et al. (2013). New radar interferometric time series analysis toolbox released. *Eos, Transactions American Geophysical Union*, 94(7), 69–70. doi: 10.1002/2013EO070001
- Amelung, F., Galloway, D. L., Bell, J. W., Zebker, H. A., & Lacznik, R. J. (1999). Sensing the ups and downs of Las Vegas: InSAR reveals structural control of land subsidence and aquifer-system deformation. *Geology*, 27(6), 483–486. doi: 10.1130/0091-7613(1999)027<0483:STUADO>2.3.CO;2
- American Society of Civil Engineers. (2017). ASCE 2017 Infrastructure Report Card (Tech. Rep.). Retrieved from <https://www.infrastructurereportcard.org/cat-item/levees/>
- Bates, M. E., & Lund, J. R. (2013). Delta subsidence reversal, levee failure, and aquatic habitat—a cautionary tale. *San Francisco Estuary and Watershed Science*, 11(1). doi: 10.15447/sfews.2013v11iss1art1

- Bekaert, D., Walters, R., Wright, T., Hooper, A., & Parker, D. (2015). Statistical comparison of InSAR tropospheric correction techniques. *Remote Sensing of Environment*, 170, 40–47. doi: 10.1016/j.rse.2015.08.035
- Bekaert, D. P., Jones, C. E., An, K., & Huang, M.-H. (2019). Exploiting UAVSAR for a comprehensive analysis of subsidence in the Sacramento Delta. *Remote Sensing of Environment*, 220, 124–134. doi: 10.1016/j.rse.2018.10.023
- Berardino, P., Fornaro, G., Lanari, R., & Sansosti, E. (2002). A new algorithm for surface deformation monitoring based on small baseline differential SAR interferograms. *IEEE Transactions on Geoscience and Remote Sensing*, 40(11), 2375–2383. doi: 10.1109/TGRS.2002.803792
- Blewitt, G., Kreemer, C., Hammond, W. C., & Goldfarb, J. M. (2013). Terrestrial reference frame NA12 for crustal deformation studies in North America. *Journal of Geodynamics*, 72, 11–24. doi: 10.1016/j.jog.2013.08.004
- Boryan, C., Yang, Z., Mueller, R., & Craig, M. (2011). Monitoring U.S. agriculture: the U.S. department of agriculture, national agricultural statistics service, cropland data layer program. *Geocarto International*, 26(5), 341–358. doi: 10.1080/10106049.2011.562309
- Broadbent, F. E., et al. (1960). Factors influencing the decomposition of organic soils of the California delta. *Hilgardia*, 29, 587–612. doi: 10.3733/hilg.v29n13p587
- Brooks, B. A, Bawden, G., Manjunath, D., Werner, C., Knowles, N., Foster, J., et al. (2012). Contemporaneous Subsidence and Levee Overtopping Potential, Sacramento-San Joaquin Delta, California. *San Francisco Estuary and Watershed Science*, 10(1). Retrieved from <https://escholarship.org/uc/item/15g1b9tm>
- Buchanan, M. K., Kopp, R. E., Oppenheimer, M., & Tebaldi, C. (2016). Allowances for evolving coastal flood risk under uncertain local sea-level rise. *Climatic Change*, 137(3-4), 347–362. doi: 10.1007/s10584-016-1664-7
- CalFed Bay-Delta Program (1999). Ecosystem Restoration Program Plan Vol. 1 - Ecological Attributes of the San Francisco Bay-Delta Watershed. Programmatic EIS/EIR Technical Appendix. California Agencies. 345. Retrieved from https://digitalcommons.law.ggu.edu/caldocs_agencies/345
- California Department of Water Resources, Delta-Suisun Marsh office (2007). 2007 Sacramento San Joaquin Delta LiDAR Acquisition. Retrieved from <http://gisarchive.cnra.ca.gov/iso/ImageryBaseMapsLandCover/LIDAR/DeltaLIDAR2007/>
- California Department of Water Resources, Delta-Suisun Marsh office (2017). 2017 Sacramento San Joaquin Delta LiDAR Acquisition. Retrieved from <http://gisarchive.cnra.ca.gov/iso/ImageryBaseMapsLandCover/LIDAR/DeltaLIDAR2017/>
- Chase, A. F., Chase, D. Z., Fisher, C. T., Leisz, S. J., & Weishampel, J. F. (2012). Geospatial revolution and remote sensing LiDAR in Mesoamerican archaeology. *Proceedings of the National Academy of Sciences*, 109(32), 12916–12921. doi: 10.1073/pnas.1205198109

- Chaussard, E., Wdowinski, S., Cabral-Cano, E., & Amelung, F. (2014). Land subsidence in central Mexico detected by ALOS InSAR time-series. *Remote Sensing of Environment*, 140, 94–106. doi: 10.1016/j.rse.2013.08.038
- Deverel, S. J., Bachand, S., Brandenberg, S. J., Jones, C. E., Stewart, J. P., & Zimmaro, P. (2016). Factors and processes affecting delta levee system vulnerability. *San Francisco Estuary and Watershed Science*, 14(4). doi: 10.15447/sfew.2016v14iss4art3
- Deverel, S. J., Ingram, T., & Leighton, D. (2016). Present-day oxidative subsidence of organic soils and mitigation in the Sacramento-San Joaquin Delta, California, USA. *Hydrogeology Journal*, 24(3), 569–586. doi: 10.1007/s10040-016-1391-1
- Dixon, T. H., Amelung, F., Ferretti, A., Novali, F., Rocca, F., Dokka, R., et al. (2006). Subsidence and flooding in New Orleans. *Nature*, 441(7093), 587. doi: 10.1038/441587a
- Doin, M.-P., Lasserre, C., Peltzer, G., Cavalière, O., & Doubre, C. (2009). Corrections of stratified tropospheric delays in SAR interferometry: Validation with global atmospheric models. *Journal of Applied Geophysics*, 69(1), 35–50. doi: 10.1016/j.jappgeo.2009.03.010
- Dubayah, R. O., & Drake, J. B. (2000). Lidar remote sensing for forestry. *Journal of Forestry*, 98(6), 44–46. doi: 10.1093/jof/98.6.44
- Fore, A. G., Chapman, B. D., Hawkins, B. P., Hensley, S., Jones, C. E., Michel, T. R., & Muellerschoen, R. J. (2015). UAVSAR polarimetric calibration. *IEEE Transactions on Geoscience and Remote Sensing*, 53(6), 3481–3491. doi: 10.1109/TGRS.2014.2377637
- Global Construction Review (2016, September). Ho Chi Minh City to spend \$4.4bn to keep its head above water. Retrieved from <http://www.globalconstructionreview.com/news/ho-chi-minh-city-spend-44bn-keep-i7ts-he7ad-abo7ve/>
- Hanssen, R. F. (2001). Radar interferometry: data interpretation and error analysis (Vol. 2). *Springer Science and Business Media*. doi: 10.1007/0-306-47633-9
- Hooper, A., Zebker, H., Segall, P., & Kampes, B. (2004). A new method for measuring deformation on volcanoes and other natural terrains using InSAR persistent scatterers. *Geophysical Research Letters*, 31(23). doi: 10.1029/2004GL021737
- Ingebritsen, S., Ikehara, M., Galloway, D., & Jones, D. (2000). Delta subsidence in California: the sinking heart of the state (Tech. Rep.). Retrieved from <https://pubs.usgs.gov/fs/2000/fs00500/>
- Jaboyedoff, M., Oppikofer, T., Abellaacute;n, A., Derron, M.-H., Loye, A., Metzger, R., & Pedrazzini, A. (2012). Use of LIDAR in landslide investigations: a review. *Natural Hazards*, 61(1), 5–28. doi: 10.1007/s11069-010-9634-2
- Jones, C. E., An, K., Blom, R. G., Kent, J. D., Ivins, E. R., & Bekaert, D. (2016). Anthropogenic and geologic influences on subsidence in the vicinity of New Orleans, Louisiana. *Journal of Geophysical Research: Solid Earth*, 121(5), 3867–3887. doi: 10.1002/2015JB012636
- Jones, C. E., Dudas, J., & Bawden, G. W. (2016). Application of Remote Sensing to Assessment of Water Conveyance Infrastructure Integrity. *Applied Geology in California, Environmental Engineering Geologists*, 26, 253–271.

- Kulp, S. A., & Strauss, B. H. (2019). New elevation data triple estimates of global vulnerability to sea-level rise and coastal flooding. *Nature Communications*, 10(1), 1–12. doi: 10.1038/s41467-019-12808-z
- Lanari, R., Lundgren, P., Manzo, M., & Casu, F. (2004). Satellite radar interferometry time series analysis of surface deformation for Los Angeles, California. *Geophysical Research Letters*, 31(23). doi: 10.1029/2004GL021294
- Lim, M. (2018, March). Seven years after tsunami, Japanese live uneasily with seawalls. Retrieved from <https://www.reuters.com/article/us-japan-disaster-seawalls/seven-years-after-tsunami-japanese-live-uneasily-with-seawalls-idUSKCN1GL0DK>
- Lund, J. R. (2016). California's agricultural and urban water supply reliability and the Sacramento–San Joaquin Delta. *San Francisco Estuary and Watershed Science*, 14(3). doi: 10.15447/sfews.2016v14iss3art6
- Luoma, S. N., Dahm, C. N., Healey, M., & Moore, J. N. (2015). Challenges facing the Sacramento–San Joaquin Delta: complex, chaotic, or simply cantankerous? *San Francisco Estuary and Watershed Science*, 13(3). doi: 10.15447/sfews.2015v13iss3art7
- Markus, T., Neumann, T., Martino, A., Abdalati, W., Brunt, K., Csatho, B., et al. (2017). The Ice, Cloud, and land Elevation Satellite-2 (ICESat 2): science requirements, concept, and implementation. *Remote Sensing of Environment*, 190, 260–273. doi: 10.1016/j.rse.2016.12.029
- McGranahan, G., Balk, D., & Anderson, B. (2007). The rising tide: Assessing the risks of climate change and human settlements in low elevation coastal zones. *Environment and Urbanization*, 19(1), 17–37. doi: 10.1177/0956247807076960
- National Academies of Sciences, E., & Medicine. (2018). Thriving on our changing planet: A decadal strategy for earth observation from space. Washington, DC: The National Academies Press. Retrieved from <https://www.nap.edu/catalog/24938/thriving-on-our-changing-planet-a-decadal-strategy-for-earth>. doi: 10.17226/24938
- Özer, I. E., van Leijen, F. J., Jonkman, S. N., & Hanssen, R. F. (2019). Applicability of satellite radar imaging to monitor the conditions of levees. *Journal of Flood Risk Management*, 12(S2), e12509. doi: 10.1111/jfr3.12509
- Prokopovich, N. P. (1985). Subsidence of peat in California and Florida. *Bulletin of the Association of Engineering Geologists*, 22(4), 395–420. doi: 10.2113/gsegeosci.xxii.4.395
- Reinert, E., Stewart, J. P., Moss, R. E., & Brandenberg, S. J. (2014). Dynamic response of a model levee on Sherman Island peat: A curated data set. *Earthquake Spectra*, 30(2), 639–656. doi: 10.1193/101913EQS274M
- Rojstaczer, S., & Deverel, S. J. (1993). Time dependence in atmospheric carbon inputs from drainage of organic soils. *Geophysical Research Letters*, 20(13), 1383–1386. doi: 10.1029/93GL01339
- Rosen, P., Hensley, S., Shaffer, S., Edelstein, W., Kim, Y., Kumar, R., et al. (2017). The NASA-ISRO SAR (NISAR) mission dual-band radar instrument preliminary design. *2017 IEEE*

- International Geoscience and Remote Sensing Symposium (IGARSS)*, 3832–3835. doi: 10.1109/IGARSS.2017.8127836
- Schmidt, C. W. (2015). Delta subsidence: An imminent threat to coastal populations. *Environmental Health Perspectives*, 123, 204–209. doi: 10.1289/ehp.123-A204
- Sehat, S., Vahedifard, F., Aanstoos, J. V., Dabbiru, L., Hasan, K., & Mooney, M. A. (2014). Analysis of the Output from a Radar-Based Levee-Monitoring System Using In Situ Soil Data. In *Geo-congress 2014: Geo-characterization and Modeling for Sustainability* (pp. 943–952). doi: 10.1061/9780784413272.092
- Service, R. F. (2007). Environmental restoration. Delta blues, California style. *Science*, 317(5837), 442. doi: 10.1126/science.317.5837.442
- Syvitski, J. P., Kettner, A. J., Overeem, I., Hutton, E. W., Hannon, M. T., Brakenridge, G. R., et al. (2009). Sinking deltas due to human activities. *Nature Geoscience*, 2(10), 681. doi: 10.1038/ngeo629
- Tebaldi, C., Strauss, B. H., & Zervas, C. E. (2012). Modelling sea level rise impacts on storm surges along US coasts. *Environmental Research Letters*, 7(1), 014032. doi: 10.1088/1748-9326/7/1/014032
- Tessler, Z., Vörösmarty, C. J., Grossberg, M., Gladkova, I., Aizenman, H., Syvitski, J., & Foufoula-Georgiou, E. (2015). Profiling risk and sustainability in coastal deltas of the world. *Science*, 349(6248), 638–643. doi: 10.1126/science.aab3574
- USACE. (n.d.). National Levee Safety - Levee Situation in the U.S. (Tech. Rep.). Retrieved from <https://www.usace.army.mil/National-Levee-Safety/About-Levees/Levee-Situation-in-the-US/>
- Weir, W. W. (1950). Subsidence of peat lands of the Sacramento-San Joaquin delta, California. *Hilgardia*, 20, 37–56. doi:10.3733/hilg.v20n03p037
- The World Bank (2017, September). Project Highlights: Metro Manila Flood Management. Retrieved from <https://www.worldbank.org/en/country/philippines/brief/project-highlights-metro-manila-flood-management>
- Wuebbles, D. J., Fahey, D. W., & Hibbard, K. A. (2017). USGCRP, 2017: Climate Science Special Report: Fourth National Climate Assessment, Volume I (Vol. 1; Tech. Rep.). Retrieved from <https://science2017.globalchange.gov/>
- Younes, S. A.-M. (2016). Modeling investigation of wet tropospheric delay error and precipitable water vapor content in Egypt. *The Egyptian Journal of Remote Sensing and Space Science*, 19(2), 333–342. doi: 10.1016/j.ejrs.2016.05.002
- Zebker, H. A., & Villasenor, J. (1992). Decorrelation in interferometric radar echoes. *IEEE Transactions on Geoscience and Remote Sensing*, 30(5), 950–959. doi: 10.1109/36.175330

1
2
3
4
5
6
7
8
9
10
11
12
13
14
15
16
17
18
19
20
21
22
23
24
25
26
27
28
29

[Earth and Space Science]

Supporting Information for

[Radar interferometry offers new monitoring approach for critical flood control infrastructure]

[K. An¹, C. E. Jones², D. P. S. Bekaert² and V. Bennett³]

¹ Department of Geography, University of California, Los Angeles, Los Angeles, CA 90095, USA.

² Jet Propulsion Laboratory, California Institute of Technology, Pasadena, CA 91109, USA.

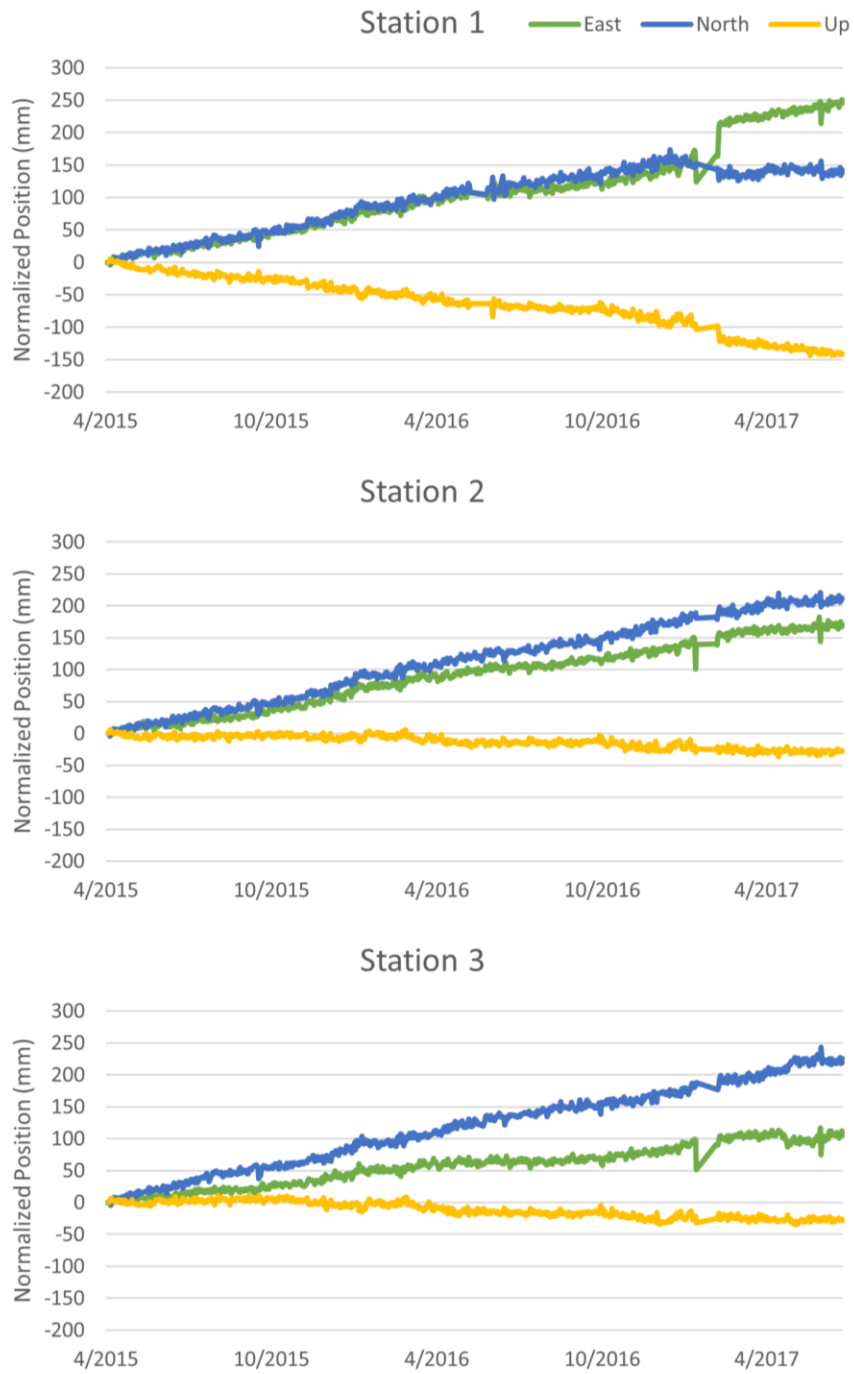
³ Department of Civil and Environmental Engineering, Rensselaer Polytechnic Institute, Troy, NY 12180, USA.]

Contents of this file

Figures S1 to S7

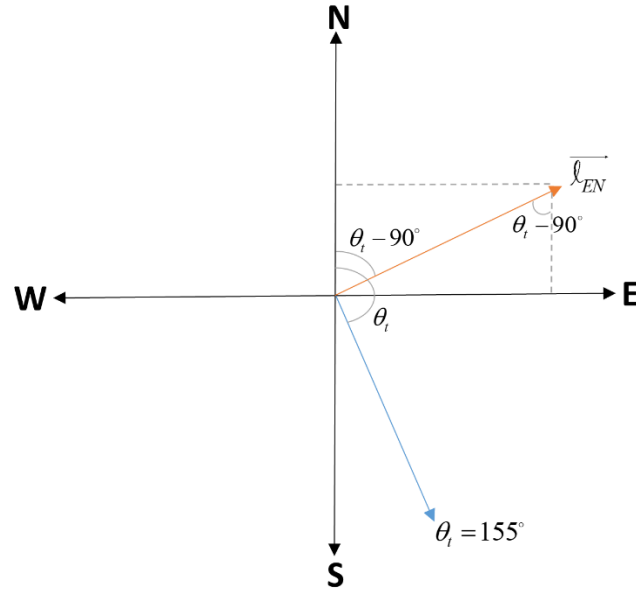
Introduction

The original raw GPS time series is shown for all three stations on Sherman Island, as well as a schematic of the GPS data conversion to the line-of-sight. Overview figures of vertical velocity and vertical velocity uncertainty are provided for the major Delta islands. In addition, a figure on the sensitivity analysis between the InSAR and lidar datasets is shown. An example of how the levee oriented moving window was generated is also shown. Lastly, 20 more examples of historic levee breaks are included which exceeded space in the paper.]



30
31
32
33
34
35
36
37

Figure S1. Original GPS time series. Raw time series (including data jumps) for the Sherman test site stations (locations shown in Fig. 2C). Positional change is normalized to the first data entry for visualization.



38

39

$$\begin{aligned} l_E &= l_{EN} \sin(\theta_i - 90^\circ) \\ l_N &= l_{EN} \cos(\theta_i - 90^\circ) \end{aligned} \quad (1)$$

$$\hat{l} = \frac{\vec{l}}{l}$$

40

$$\begin{aligned} \hat{l} &= -\cos \theta_i \hat{U} + \sin \theta_i \cos(\theta_i - 90^\circ) \hat{N} + \sin \theta_i \sin(\theta_i - 90^\circ) \hat{E} \\ \vec{l} &= -l \cos \theta_i \hat{U} + l \sin \theta_i \cos(\theta_i - 90^\circ) \hat{N} + l \sin \theta_i \sin(\theta_i - 90^\circ) \hat{E} \end{aligned} \quad (2)$$

41

$$\begin{aligned} \vec{d}_{GPS} &= d_U \hat{U} + d_N \hat{N} + d_E \hat{E} \\ \vec{d} \cdot \hat{l} &= -[d_U (-\cos \theta_i) + d_N \sin \theta_i \cos(\theta_i - 90^\circ) + d_E \sin \theta_i \sin(\theta_i - 90^\circ)] \end{aligned} \quad (3)$$

42

43

44

45

46

47

48

49

50

51

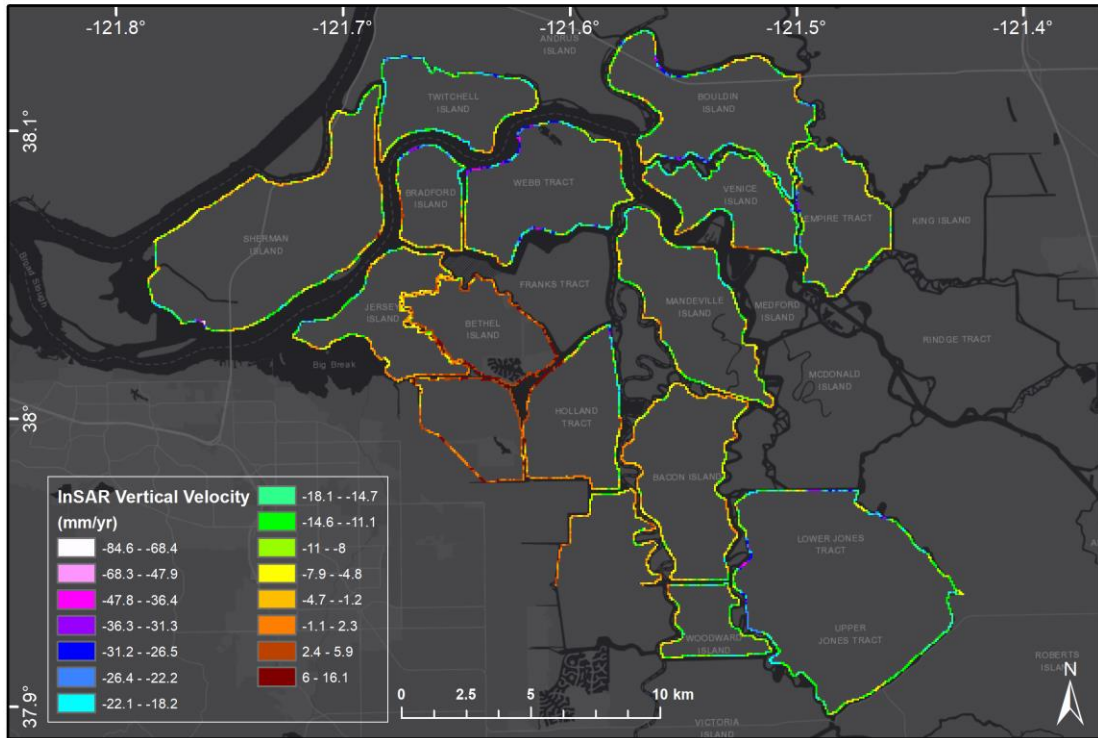
52

53

54

55

Figure S2. GPS-LOS conversion. A schematic of the projected east-north component for UAVSAR flight line 15502 where θ_i is the track angle from north and \vec{l}_{EN} is the east-north vector. Eq. 1 shows the individual east and north components in terms of the east-north vector and the track angle. Eq. 2 solves for the unit vector \hat{l} by dividing the vector \vec{l} by its length l . The unit vector is shown in terms of its east, north, and up vectors where θ_i is the incidence angle. Eq. 3 shows the GPS displacement vector in terms of its east, north, and up components. The dot product between this displacement vector and the unit vector is solved to convert the GPS positions to the UAVSAR line-of-sight displacements. A final negative is taken of this equation because the GIANt program assigns the look direction as positive looking up from the target. The converted LOS values are shown in Fig. 2E.



56
57
58
59
60
61
62
63
64
65
66
67
68
69
70
71
72
73
74
75
76
77
78
79
80
81

Figure S3. Overview vertical velocity map. Vertical velocity for the central and western Delta islands where blue and purple denote subsidence and orange and red areas show more stable or uplift areas. Pixel size is enlarged to 70 m for better visibility.

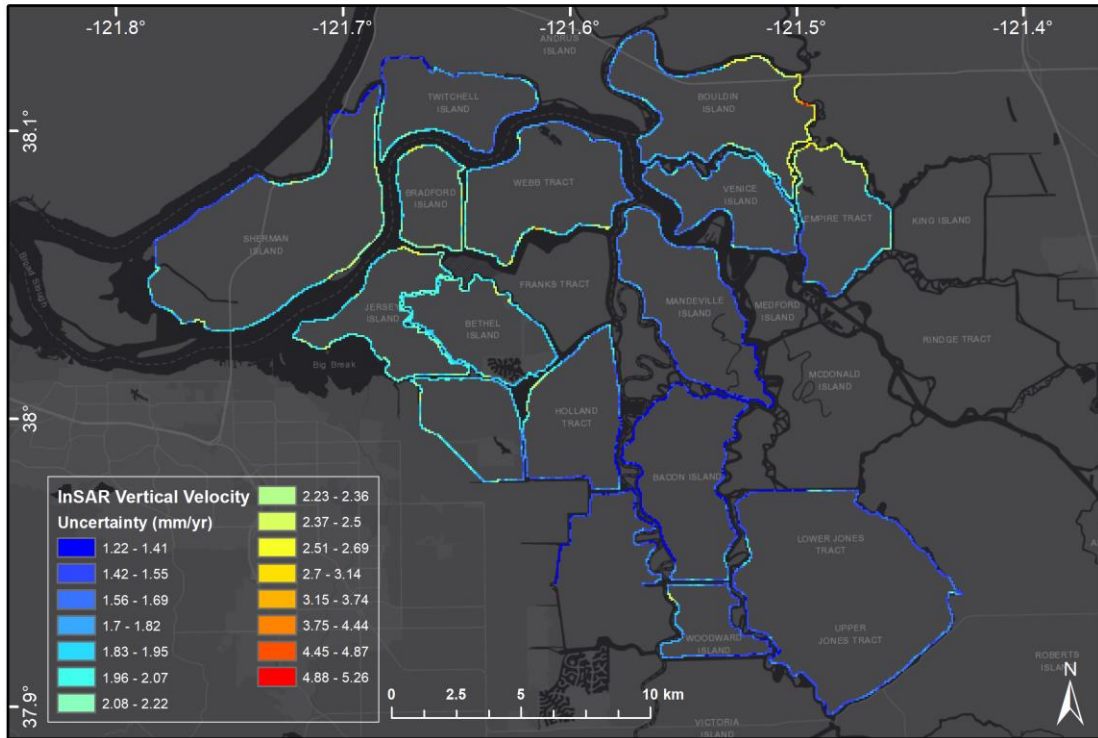
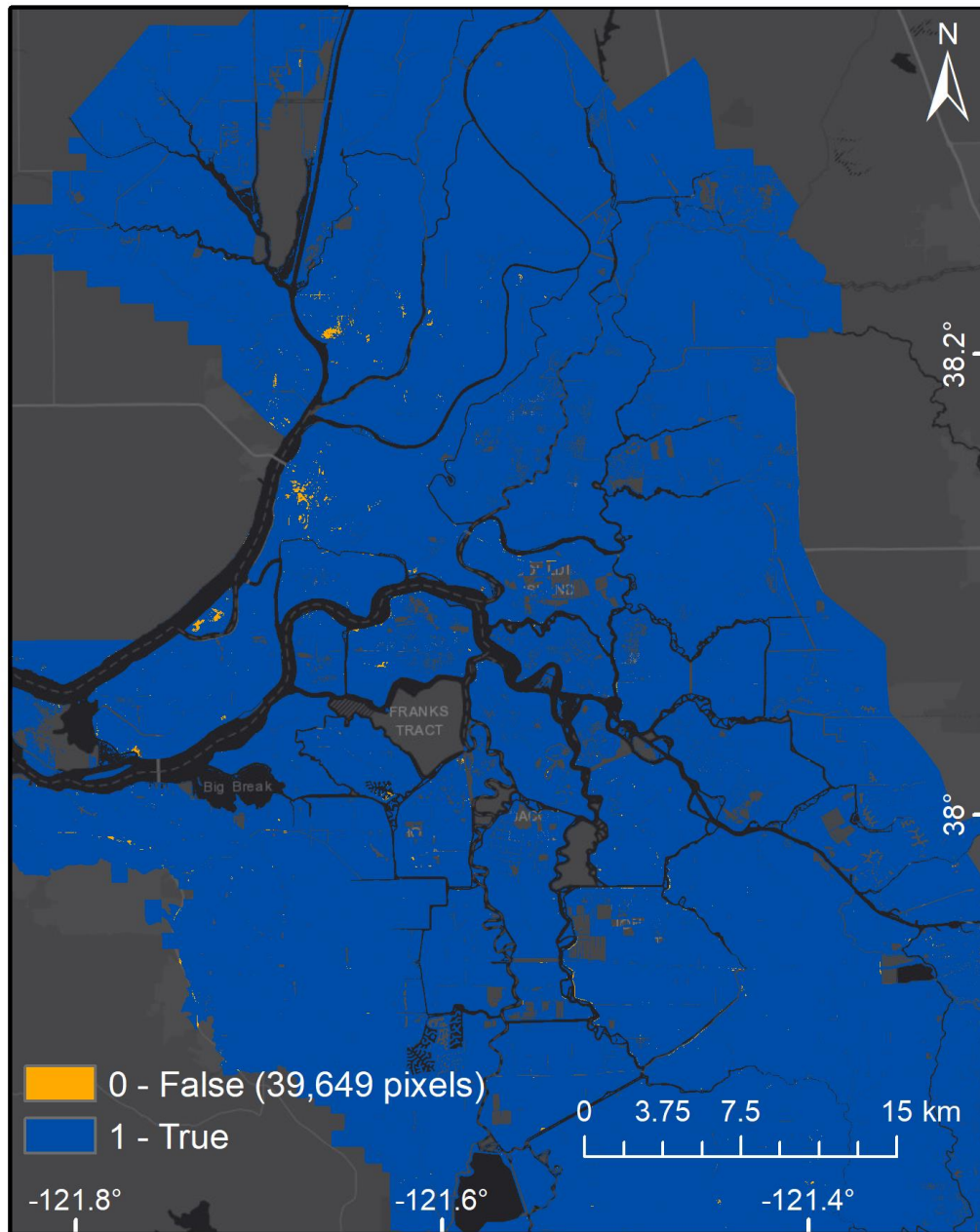


Figure S4. Overview uncertainty map. Vertical velocity uncertainty values for the central and western Delta islands where blue and purple denote lower uncertainty and orange and red areas show more uncertainty. Pixel size is enlarged to 70 m for better visibility.

82
83
84
85
86
87
88
89
90
91
92
93
94
95
96
97
98
99
100
101
102
103
104
105
106
107
108

$$\text{Sensitivity Expression: } |InSAR - Lidar| \leq \sqrt{\sigma^2_{InSAR} - \sigma^2_{Lidar}}$$



109

110

111

112

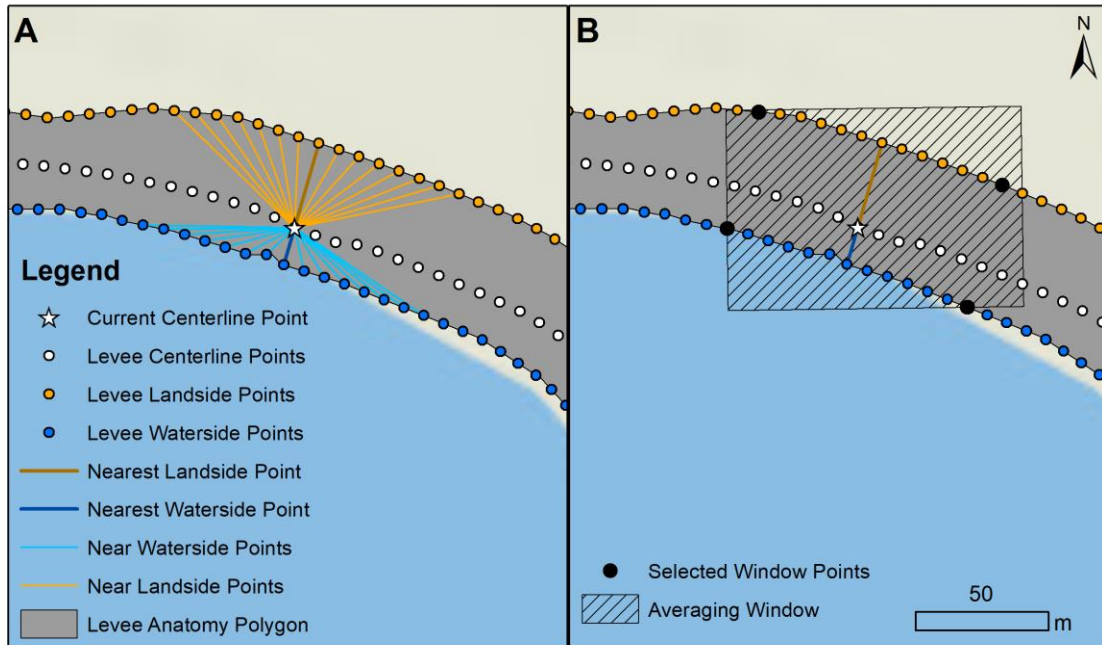
113

114

115

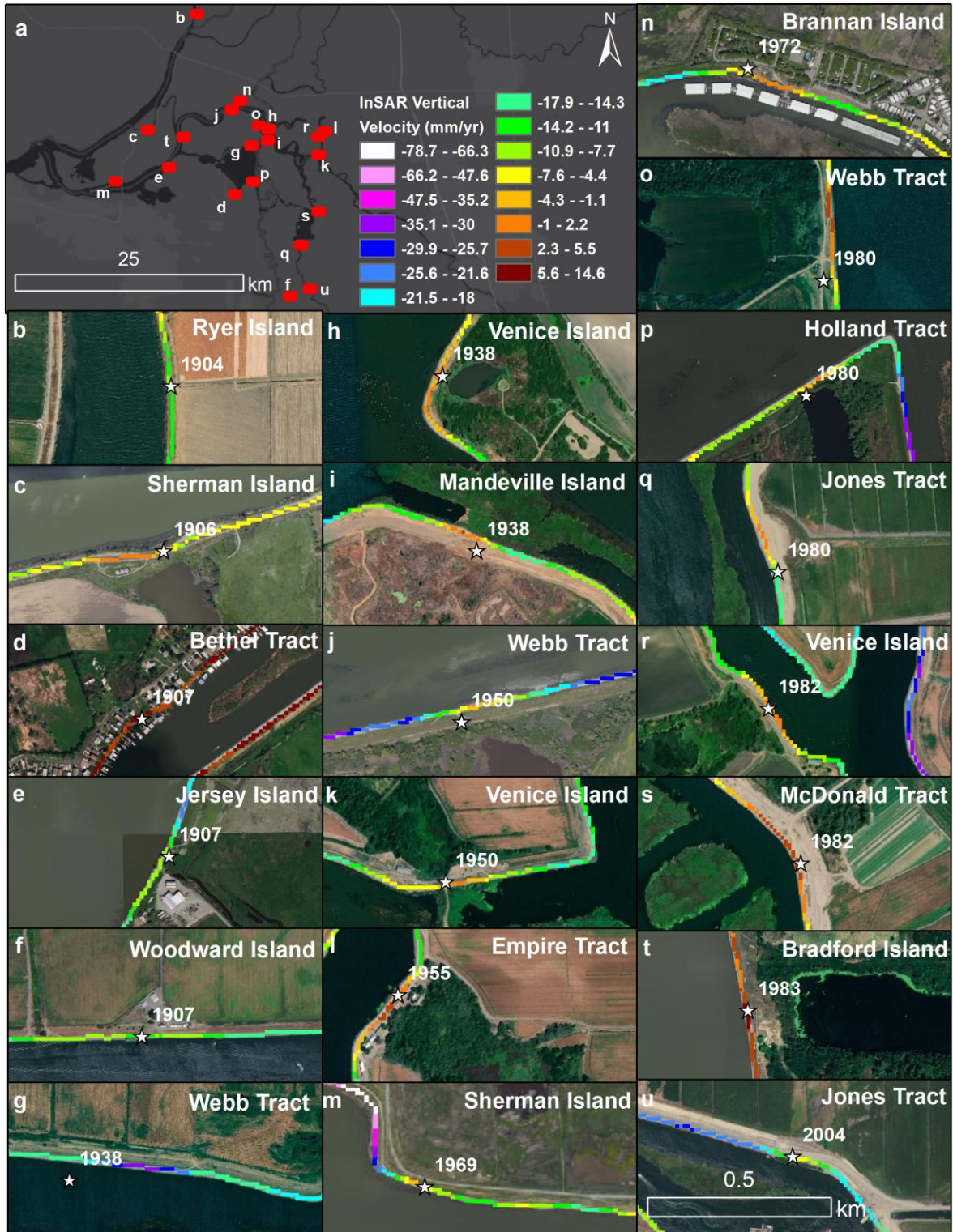
116

Figure S5. Sensitivity analysis. The sensitivity between the InSAR and lidar datasets was calculated using the above expression, where σ_{InSAR} is the 1-sigma uncertainty calculated for the InSAR vertical velocity rates (see Bekaert, et al. 2019) and σ_{LiDAR} is 10.7 mm/yr, which is the 1-sigma uncertainty as calculated from the 95% confidence level values for vertical accuracy reported from the lidar datasets. Orange pixels show areas where the difference between InSAR and lidar is not within uncertainty bounds, and blue pixels show areas where the datasets are within each other's 1-sigma uncertainty bounds.



117
 118
 119
 120
 121
 122
 123
 124
 125
 126
 127
 128
 129
 130
 131
 132
 133
 134
 135
 136
 137
 138
 139
 140
 141
 142
 143
 144
 145

Figure S6. Levee oriented moving window average. (a) An example levee section on southwest Sherman Island showing the levee centerline (white), landside (orange), and waterside (blue) points generated from the levee anatomy polygon (grey). While working on the current centerline point (white star), the nearest landside and waterside points are located. (b) Counting six points away on both sides from the nearest landside and waterside points, the window border points of the averaging window are chosen (black). Based on these window points, a best-fit averaging window is generated.



146
147
148
149

Figure S7. More historic levee breaks. (a) Overview of the Sacramento-San Joaquin Delta with locations of all levee breaks (red). (b-u) Vertical velocities showing more stable conditions at historic levee break throughout the Delta.